JOURNAL OF CATALYSIS **163,** 476–488 (1996)
ARTICLE NO. 0349

Amorphous Microporous Titania–Silica Mixed Oxides: Preparation, Characterization, and Catalytic Redox Properties

S. Klein, S. Thorimbert, and W. F. Maier[1]

Max-Planck-Institut für Kohlenforschung, Kaiser-Wilhelm-Platz 1, D-45470, Mülheim a.d. Ruhr, Germany

Received March 4, 1996; revised May 21, 1996; accepted May 28, 1996

Microporous titania–silica mixed oxides with a narrow monomodal pore size distribution at pore diameters of 0.7 nm with highly dispersed titanium in the silica matrix have been obtained by a simple acid-catalyzed sol–gel process in the absence of chelating agents or the prehydrolysis techniques. A mixture of titanium(IV)alkoxide and tetraethoxysilane (TEOS) has been hydrolysed in alcoholic solution with aqueous hydrochloric acid followed by calcination, resulting in amorphous, microporous mixed oxides. There is no limitation on the chemical composition, which covers the whole range from microporous silica to microporous titania. The structural and chemical properties of the materials as a function of preparation parameters (such as acid, titania, or water content, respectively, nature of alcohol, gelation temperature, drying conditions, and titanium source) have been studied by means of physisorption (Ar and N_2), X-ray powder diffraction, spectroscopic techniques, high resolution TEM (in combination with EDX and electron diffraction) and catalytic test reactions (epoxidation of olefins, selective oxidations of saturated hydrocarbons). The high Ti dispersion was negatively affected by changes in the Ti source and/or the alcohol used for the sol–gel process. Increasing BET surface areas were detected as function of the Si/Ti ratio at an optimum in acid concentration. The Si-excess materials stayed X-ray amorphous up to 1173 K. FTIR studies after pyridine treatment showed the materials having weak acidity only. With increasing Ti content an increase in Ti–O–Ti connectivity is observed by DRIFT spectroscopy, resulting in a decrease in epoxidation activity. The glasses show not only catalytic activity for selective oxidation reactions with TBHP comparable with that of other titania containing materials, but size selective epoxidations of olefins are interpreted as shape selectivity resulting from their distinct microporosity. Competitive adsorption experiments of water and octane suggest the hydrophilicity of the amorphous oxides to be the major difference in comparison to their zeolitic analogues.

INTRODUCTION

During the past two decades amorphous glasses prepared by the sol–gel process experienced a rapid development (1–3). Simultaneously the chemistry of the sol–gel process advanced significantly (1, 4). This hydrolysis–polycondensation reaction of metal-alkoxides has been subject of numerous mechanistic and structural investigations (2, 5–7). A growing number of applications, such as coating, thin films, glasses with low thermal expansion coefficient (8, 9), and precursors for the preparation of ceramic materials (10, 11), have been reported. Although a modified sol–gel step is often part of modern zeolite syntheses (12), the use of sol–gel derived materials as catalyst supports (13, 14) or catalysts (15–18) is still in its infancy. The broad variability of the sol–gel method allows not only potential fine tuning of material properties such as chemical composition and tailored surface structure by molecular imprinting (19), but also the design of shape and texture of the final products like films and coatings (3, 20, 21) crack-free (22) or nonshrinking (23) monoliths, fibers or membranes (24, 25). The preparation of microporous silica, alumina, zirconia, and titania with a narrow monomodal pore size distribution via the sol–gel process has been reported (26). Membranes made from these sols were shown to exhibit gas and liquid separation properties for small molecules (27). Selective catalytic epoxidation properties of such materials based on titaniumcyclopentadienyldichloride derived silica glasses have been reported (28). This same precursor was later used to prepare an MCM-based epoxidation catalyst (29). We could also show that microporous mixed Ti–Si glasses exhibit shape selective properties in the decane hydrocracking test and in epoxidation reactions with TBHP (30).

Ti-based selective heterogeneous redox catalysis originated in the discovery of the selective oxidation properties of titania on silica, utilized in the SHELL-catalyst for the selective oxidation of propene to propylene oxide with ethylbenzene hydroperoxide (31). This material is obtained by hydrolysis of titanium chloride species grafted to a silica surface resulting in small titania domains on a silica carrier. This epoxidation is limited to the use of organic hydroperoxides as oxidating agents and the development of more versatile epoxidation catalysts remained a desirable goal (32). The discovery of the Ti-containing silicalite TS-1 (MFI-structure) allowed the use of environmentally friendly H_2O_2 as the oxidant for selective oxidation (33). It

[1] To whom correspondence should be addressed. E-Mail: maier@dsa.mpi-muelheim.mpg.de.

0021-9517/96 $18.00

initiated the development of a variety of new zeolytic materials, such as TS-2 (MEL-structure) (34), Ti-beta (35) or Ti-MCM-41 (36), in which isomorphic substitution of Si by Ti provides a growing family of selective oxidation catalysts (37–39). Isomorphic substitution of Si by Ti in the framework is held responsible for the unique selectivities of these crystalline catalysts.

Amorphous binary Ti–Si oxides have been investigated even longer than the Ti-zeolites and numerous studies inform us about surface acidity (12, 40–44), microstructural properties (45–47), and the particulars in sol–gel processes involving titanium alkoxides (48–51). Domain formation due to reactivity differences between Ti- and Si alkoxides was identified as a major problem in the preparation of the mixed oxides. Prehydrolysis (52, 53) of the less reactive Si-species and modification of the highly labile Ti-alkoxides by means of chelation (54–59) have often been proposed in order to compensate for the differences in hydrolysis and condensation rates of these compounds. However, very few studies examined the properties of amorphous Ti–Si oxides in oxidation catalysis and its correlation with the materials structure. In all these crystalline and amorphous systems, the presence of site-isolated $Ti(OSi)_4$ species seems to be crucial for the oxidation reactions reported (60), favoring the sol–gel approach in the synthesis of binary mixed oxides with high homogeneity in chemical composition.

The preparation of mesoporous amorphous titania–silica mixed oxides with total surfaces of several hundred m^2/g by a carefully developed sol–gel process was recently reported (61–63). During the preparation of these aerogels special attention was paid to the generation of site isolated Ti by combining Ti alkoxide chelation, Si alkoxide prehydrolysis, and supercritical drying techniques. The effort paid off, since these materials are highly active and selective epoxidation catalysts for bulky olefins. These mesoporous Ti-catalysts not only expand the range of selective oxidation catalysts, they also illustrate the potential of the sol–gel process for the preparation of novel catalyst materials based on site isolated centers in amorphous silica matrices. While these aerogel materials are free of micropores we report here the preparation and characterization of amorphous microporous titania–silica mixed oxides, prepared by an alternative acid catalyzed sol–gel procedure.

In the past we had optimized the sol–gel process to provide amorphous oxides with a stable monomodal narrow micropore distribution (26). The final sol–gel procedure is remarkably simple, it avoids expensive chelating agents, pressurized drying techniques, and complicated preparation procedures or hydrothermal processing. Rheological studies on the reaction mixture at the sol–gel transition showed that under acidic conditions elasticity increases more rapidly than viscosity, indicating a linear polycondensation mechanism (64). It was already recognized that acidic sol–gel conditions are most promising to obtain high Si–O–Ti connectivities (50). This is readily understood by the reaction mechanism, where attack of the proton occurs at the oxygen atom of alkoxide bonds. Thus the nucleophilicity differences of the central atoms, which cause domain formation at basic sol–gel conditions, has little influence on the polycondensation process under acid catalysis.

Our aim was to optimize our simple sol–gel route to provide atomically dispersed mixed oxides while maintaining the narrow micropore distribution from the preparation of the pure oxides. While pore size distribution of the products is readily monitored by sorption experiments, our routine HRTEM studies provide only information about amorphicity and elemental homogeneity. To obtain additional information supporting the desired atomic dispersion various spectroscopic techniques (FTIR, UV/VIS-DRS, XANES) had to supplement the routine characterization methods. Such amorphous microporous Ti–Si-mixed oxides not only supplement the above mentioned mesoporous materials, but are alternative materials to the microporous Ti-zeolites. Independent of all structural characterization only the comparison of the catalytic performance of these amorphous oxides in selective epoxidation of alkenes with the well described performance of the crystalline Ti-zeolites allows to judge the usefulness of these new materials in catalysis.

METHODS

The materials described here are further denoted as AMM-Ti_xSi, with AMM abbreviating amorphous microporous mixed oxide, where x gives the mol% of TiO_2 in the mixed oxide, and Si represents SiO_2 as matrix material.

Preparation of the Gels

The recipe (optimized for narrow micropore distribution and atomic dispersion) of preparation used for the majority of samples is based on the preparation of the pure amorphous oxides already mentioned in the introduction (26, 27).

Sol–gel process. This standard sol–gel procedure is using the substances in the molar ratios of tetraethoxysilane (TEOS): tetraalkoxytitanium ($Ti(OR)_4$) : H_2O : HCl : R–OH = $x : y : 2(x + y) : 0.35(x + y) : 3(x + y)$, where x and y range between 0 and 1 and R for the alcohol and alkoxide used respectively is ethyl or *i*-propyl. The amount of (Si-alkoxide + Ti-alkoxide) used usually is 50 mmol. The substance ratios have been modified in order to examine the influence of water and acid content on the gel properties. In the case of altering the water content, the amount of acid was kept constant and vice versa. This was achieved by using acids of varying concentrations instead of 8 mol/liter HCl or extra water.

If not mentioned explicitly, the standard procedure was the following: TEOS is placed in a 100-ml PP beaker

TABLE 1

Quantities and Chemical Composition of the Catalysts Prepared under Standard Conditions

Material	Ratio Si/Ti	mmol TIPOT[a]	mmol TEOS	mmol R–OH	mmol HCl	mmol H_2O
AMM-Si	∞	0	50	150, EtOH	17.5, 8 *N*	101
AMM-Ti_1Si	100	0.5	49.5	150, EtOH	17.5, 8 *N*	101
AMM-Ti_1Si	100	0.5	49.5	150, *i*-PrOH	17.5, 8 *N*	101
AMM-Ti_1Si,TEOT[b]	100	0.5	49.5	150, EtOH	17.5, 8 *N*	101
AMM-Ti_2Si	50	1.0	49.0	150, EtOH	17.5, 8 *N*	101
AMM-Ti_2Si	50	1.0	49.0	150, *i*-PrOH	17.5, 8 *N*	101
AMM-Ti_3Si	30	1.5	48.5	150, EtOH	17.5, 8 *N*	101
AMM-Ti_5Si	17	2.5	47.5	150, EtOH	17.5, 8 *N*	101
AMM-Ti_9Si	10	4.5	45.5	150, EtOH	17.5, 8 *N*	101
AMM-Ti_{17}Si	5	8.5	41.5	150, EtOH	17.5, 8 *N*	101
AMM-Ti_{33}Si	2	16.5	33.5	150, EtOH	17.5, 8 *N*	101
AMM-Ti_{50}Si	1	25	25	150, EtOH	17.5, 8 *N*	101
AMM-Ti_{67}Si	0.5	33.5	16.5	150, EtOH	17.5, 8 *N*	101
AMM-Ti[c]	0	50	0	150, EtOH	17.5, 8 *N*	101

Note. Standard sol–gel procedure and conventional drying/calcination explained under Methods, 17.5 mmol 8*N* HCl, 101 mmol H_2O.

[a] Titanium(VI)isopropoxide (TIPOT) used if not explicitly mentioned.

[b] TEOT, Titanium(VI)ethoxide used as Ti source.

[c] Immediate precipitation occurred during addition of aqueous acid.

equipped with a magnetic stirring bar and mixed with the corresponding volume of the titanium compound. This solution is diluted with the alcohol. Subsequently, the corresponding amount of water and acid is introduced by adding aqueous HCI (8 mol HCl/liter) dropwise to the well stirred solution which turns from colourless to yellow under these conditions.

Prehydrolysis technique. To a solution of 45 mmol TEOS in 4 ml of ethanol, 1.1 ml of aqueous hydrochloric acid (8 mol/liter) in 2 ml of ethanol was added slowly via syringe under vigorous stirring. After 2 h at 298 K, a solution of tetraisopropoxytitanium (TIPOT) in 2 ml of ethanol was added dropwise. Hydrolysis was completed by a dropwise addition of 1.1 ml HCl (8 mol/liter). The clear yellow solution solidified within 2 days under stirring and was calcined according to the following standard method.

Drying and calcination procedures. The sols were subjected to the following drying/ageing and calcination conditions:

(i) Standard method: The clear solution was stirred for 5 min and then placed in the hood, loosely covered to allow slow evaporation of the volatiles. Solidification usually occurred after 3–4 days. Subsequently, the following heat treatment was applied: starting at room temperature the samples were heated up to 338 K with a rate of 0.2 K/min and kept at this temperature for a drying period of 5 h. Then, the temperature was allowed to rise at 523 K (rate of 0.5 K/min) for a period of 5 h. Finally the samples were cooled down to room temperature by 1 K/min. The procedure was finished by crushing the glasses in a ball mill for 15 min. Specific changes in the gelification, drying, and calcination procedure are described below.

(ii) Accelerated procedure: The sol–gel process could be accelerated by increasing the gelation temperature from 298 K up to 313 and 333 K, respectively. Evacuation of the gel (10^4 Pa, 12 h, 298 K) or purging dry gas (air or argon) over the material in a closed flask (3 days, 298 or 318 K) prior to the described programmed calcination resulted in further reduction of the processing time.

(iii) Decelerated procedure: In contrast to (ii), the drying period can be extended by aging the materials in open or closed flasks after gelification to retard the evaporation of the volatiles for different periods. After this slow formation of the network, the samples were calcined according to the process described in (i).

(iv) Accelerated calcination: An accelerated calcination procedure has been tested by placing the solidified gels immediately in a furnace at 523 K without smooth drying steps at lower temperatures or a ramped heating.

Table 1 displays the experimental sol–gel, drying and calcination conditions of the so-called standard materials, while specific materials produced under different conditions are listed in Table 2.

Physicochemical Characterization

Physisorptions. Physisorption isotherms were obtained routinely at 77 K on a Coulter Omnisorp 360 (argon as probe molecule, continuous flow technique in the range of $p/p_0 = 0$–0.24) or a Carlo Erba Sorptomatic 1900 (nitrogen as probe molecule, range of $p/p_0 = 0$–1), respectively. The samples were heated up to 523 K for 48 h at 5×10^{-4} Pa prior

TABLE 2

Quantities and Chemical Composition of the Catalysts Prepared under Conditions Different from the Standard Procedures

Material	Ratio Si/Ti	mmol TIPOT	mmol TEOS	mmol R–OH	mmol HCl	mmol H_2O
AMM-Ti_3Si, G313[a]	30	1.5	48.5	150, EtOH	17.5, 8 *N*	101
AMM-Ti_3Si, G333[b]	30	1.5	48.5	150, EtOH	17.5, 8 *N*	101
AMM-Ti_3Si, LAC[c]	30	1.5	48.5	150, EtOH	5.8, 8 *N*	101
AMM-Ti_3Si, HAC[d]	30	1.5	48.5	150, EtOH	52.5, 12 *N*	101
AMM-Ti_9Si, vac.[e]	10	4.5	45.5	150, EtOH	17.5, 8 *N*	101
AMM-$Ti_{17}Si$, FC[f]	5	8.5	41.5	150, EtOH	17.5, 8 *N*	101
AMM-Ti_1Si, AD[g]	100	0.5	49.5	150, *i*-PrOH	17.5, 8 *N*	101
AMM-Ti_2Si, DD[h]	50	1.0	49.0	150, *i*-PrOH	17.5, 8 *N*	101
AMM-Ti_1Si, HWR[i]	100	0.5	49.5	150, *i*-PrOH	17.5, 8 *N*	280
AMM-Ti_9Si, P[j]	10	4.5	45.5	150, EtOH	17.5, 8 *N*	101

[a] G313, gelation carried out at 313 K.
[b] G333, gelation carried out at 333 K.
[c] LAC, low acid content sol–gel process.
[d] HAC, high acid content sol–gel process, 12 mol/liter HCl required.
[e] vac., removal of the volatiles in vacuum.
[f] FC, fast calcination procedure after gelation.
[g] AD, accelerated drying, air flow, 318 K.
[h] DD, decelerated drying, gel stored in a closed flask after gelation for 2 weeks.
[i] HWR, high water recipe.
[j] P, prehydrolysis technique.

to the measurement. Micropore size distributions were calculated from Ar-adsorption isotherms with the Horváth–Kawazoe method for microporous solids. Surface areas were calculated using the BET equation in the low pressure region ($p/p_0 = 0.008$–0.01).

High Resolution Transmission Electron Microscopy (HRTEM). The glasses were examined with HRTEM on a Hitachi HF 2000 instrument combined with energy dispersive X-ray analysis (EDX). Amorphicity was examined by electron diffractions (magnification, 200 k; camera length, 0.2 m) and high resolution imaging, while elemental distribution was investigated by 20–30 selected area EDX-microanalyses with area sizes varying from 2 nm to several micrometers. The samples were crushed in an agate mortar in a methanol suspension and transferred to a holey carbon grid (copper, 3 mm diameter).

X-ray diffraction. X-ray powder diffraction (XRD) patterns were measured using the Debye–Scherrer technique on a Stoe Stadi 2/PL diffractometer using Cu $K\alpha$ radiation in the range of $2\theta = 10^\circ$–80°. The detector used was an area detector PSD 1. The temperature dependence of the patterns was examined in the temperature range from 323 to 1173 K (stepwise increase by 50 K prior to each measurements) and displayed after background correction.

UV spectroscopy. UV spectroscopy was carried out on a Varian Cary 05 UV–VIS–NIR spectrometer in diffusive reflectance technique (DRS) in the range of 12,500 to 50,000 cm^{-1} (scan rate, 25,000 cm^{-1}/min). The spectra were recorded under ambient as well as under dry conditions using a special quartz cell, which allowed heat treatment (12–15 h at 573 K in a flow of nitrogene) and measurement in moisture-free atmosphere. The Kubelka–Munk function (65) was used to display the data.

FTIR spectroscopy. Surface acidity was measured via FTIR spectroscopy after adsorption of pyridine as a probe molecule; 10 mg of the ground material was weighed in an alumina beaker and introduced into a tube reactor. Activation was carried out at 673 K for 4 h in a stream of dry argon (30 ml/min). Subsequently, a stream of argon saturated with dry pyridine (distilled and stored over KOH) was purged over the sample within 1 h at 363 K. The excess of physisorbed pyridine was removed in a flow of dry argon at 393 K within 1 h. The closed reactor was placed in a glove box, opened under inert gas, and the samples removed. The materials were placed between KBr discs (25 mm diameter) using poly-(chloro-trifluoroethylene)-oil (Merck 7450) as a suspension medium. The spectra were taken in transmittance on a Nicolet 7000 spectrometer with a spectral resolution of 2 cm^{-1} (200 scans).

Structural properties of the materials were examined with FTIR spectroscopy in diffusive reflectance (DRIFT) using a Bruker IFS 48 spectrometer equipped with a Harrick Drift unit DRA in combination with the high vacuum chamber (HVC). The ground samples were diluted with KBr and the mixture was dried *in situ* in a flow of argon at 773 K. The spectra were collected with a spectral resolution of 2 cm^{-1} (200 scans) and the experimental data displayed using the Kubelka–Munk function (dry KBr as background).

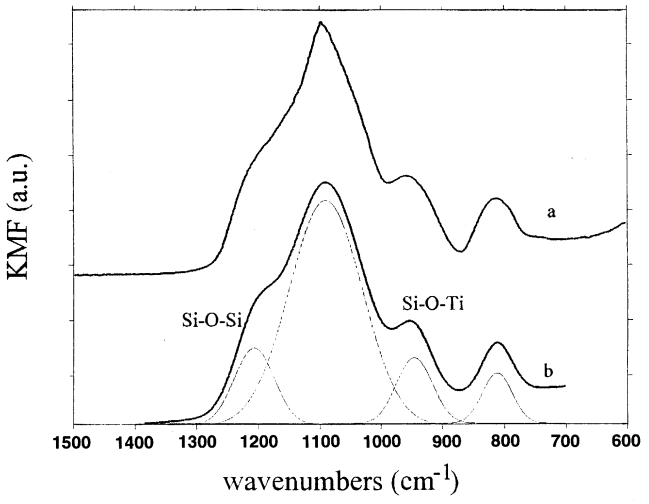

FIG. 1. DRIFTS-deconvolution using a local least square algorithm. Original spectrum (a), calculated Gauss-type signals (dotted lines), and fitted spectrum (b).

Following the accepted band assignment of 930–960 cm^{-1}, the spectral region of 750–1350 cm^{-1} has been deconvoluted into Gauss curves (Fig. 1). The <(Si–O–Si) stretching mode was chosen for comparison. The starting values for the deconvolution were 800, 950, 1100, and 1210 cm^{-1}, respectively. Width, intensity, and positions of the Gauss-type bands were optimized using the Levenberg–Marquardt local least square algorithm. According to (61), the Si–O–Ti connectivity D can be estimated following

$$D_{(\mathrm{Si-O-Ti})} = \frac{I_{(\mathrm{Si-O-Ti})}}{I_{(\mathrm{Si-O-Si})}} \cdot \frac{x_{\mathrm{Si}}}{x_{\mathrm{Ti}}} \qquad [1]$$

with I(Si–O–Ti) and I(Si–O–Si) denoting the corresponding Gauss-type integrals at 960 and 1210 cm^{-1}, respectively, and x_i equals the molar fraction of the compounds.

Hydrophobicity Measurements

Surface polarity is an important property in the use of zeolites as adsorbates. As a convenient method for characterization of this important surface property the hydrophobicity index (HI) has been developed (66). It is based on competitive adsorption experiments of water and hydrocarbons from the gas phase and allows the quanitification of the polarity of a catalyst's surface. We have carried out competetive adsorptions between water and octane under standardized conditions. The sample was placed in a tube reactor and dried *in situ* in a flow of inert gas at 673 K for 12 h. Two controlled flows of inert gas, saturated with comparable amounts of water and octane, are combined and passed over the sample at 298 K and monitored afterward by on-line GC. Evaluation of the break-through curves allows calculation of the loadings x_i and the ratio $x_{\mathrm{octane}}/x_{\mathrm{water}} = \mathrm{HI}^*$ (modified hydrophobicity index) is used as a characteristic for the hydrophobicity/hydrophilicity of the sample.

XANES Experiment

XANES experiments were carried out at the ELSA system at the University of Bonn (FRG) on AMM-Ti_3Si under ambient conditions.

Catalytic Test Reactions

Epoxidation of olefins. As a test reaction to compare the activities of the materials we carried out epoxidations of olefins with *tert*-butylhydroperoxide (TBHP). Two different methods were used depending on the desired information.

(i) Olefin (15.8 mmol) and 3 mmol of TBHP (solution in *i*-octane, 3 mol TBHP/liter ratio of olefin: TBHP, 5.3 : 1) were mixed in the presence of 50 mg of catalyst in a closed vessel. The well stirred solution was heated to 353 K.

(ii) In a modified method we have used a 1 : 1 ratio of olefin to peroxide under the following conditions: 2.4 mmol of alkene and 2.4 mmol TBHP (3 *M* solution in *i*-octane) were heated to 353 K in the presence of 25 mg catalyst. In both cases, the development of the reaction was followed by GLC. In several control experiments it was confirmed that neither pure silica, nor pure titania or a physical mixture of both were catalytically active. Furthermore, TBHP decomposition in the presence of the catalyst only as well as autooxidation of the olefin without any catalyst present can be excluded. Diffusion of smaller substrates and/or oxidizing agent is not rate limiting, since the reactions do not depend on the particle size of the catalyst. After removal of the catalyst from the mother liquor by centrifugation after a few minutes of reaction time, no further product increase could be noticed, which confirms that the AMM-Ti_xSi catalyzed reaction is heterogeneous. The reactions were carried out without precautions against moisture or oxygen.

Selective oxidations of saturated hydrocarbons. Cyclohexane was oxidized using TBHP as the oxidizing agent on different Ti-containing materials. Catalysts (20 mg) have been placed in a sealed stainless steel reactor equipped with a magnetic stirring bar. After addition of 26 mmol of TBHP (80% in di-*tert*-butylperoxide) and 31 mmol of cyclohexane, the reactor was heated in an oil bath to 353 K. Samples were taken via a sampling valve and activities/selectivities were examined by GLC.

Regeneration. The regeneration of the spent catalysts was carried out as follows: After the first reaction, the clear mother liquor was removed from the reactor after centrifugation. The remaining suspension was washed with ether and the liquid removed after centrifugation. This procedure was repeated once with ether and pentane. The dry powder was heated in an oven at 250°C for 0.5 h and used for further test reactions.

TABLE 3

Physisorption Results

Material	Ratio, Si/Ti	BET-surface area (m^2/g)	Micropore volume (cm^3/g)	Pore-size[a] diameter (nm)	Halfwidth (nm)
AMM-Si	∞	385	0.14	0.68	0.13
AMM-Ti_1Si	100	500	0.15	0.70	0.10
AMM-Ti_1Si	100	426	0.10	0.68	0.08
AMM-Ti_1Si,TEOT	100	480	0.18	0.70	0.10
AMM-Ti_2Si	50	430	0.15	0.70	0.10
AMM-Ti_2Si	50	471	0.08	0.71	0.10
AMM-Ti_3Si	30	523	0.17	0.73	0.08
AMM-Ti_5Si	17	525	0.17	0.75	0.08
AMM-Ti_9Si	10	512	0.16	0.79	0.08
AMM-Ti_{17}Si	5	395	0.13	0.76	0.06
AMM-Ti_{33}Si	2	300	0.11	0.75	0.06
AMM-Ti_{50}Si	1	300	0.11	0.86	0.05
AMM-Ti_{67}Si	0.5	162	0.05	0.65	0.10
AMM-Ti	0	100	0.05	0.80	0.15
AMM-Ti_3Si, G313	30	361	0.13	0.70	0.16
AMM-Ti_3Si, G333	30	186	0.06	0.75	0.11
AMM-Ti_3Si, LAC	30	382	0.12	0.70	0.06
AMM-Ti_3Si, HAC	30	565	0.07	0.65	0.13
AMM-Ti_9Si, vac.	10	202	0.05	0.75	0.11
AMM-Ti_{17}Si, FC	5	508	0.17	0.80	0.10
AMM-Ti_1Si, AD	100	212	0.07	0.68	0.06
AMM-Ti_2Si, DD	50	501	0.16	0.72	0.15
AMM-Ti_1Si, HWR	100	495	0.05	0.69	0.15
AMM-Ti_9Si, P	10	76	0.01	0.70	0.12

[a]Maximum of pore size distribution.

RESULTS AND DISCUSSION

Physicochemical Characterization

Physisorption. The results of the sorption measurements are listed in Table 3. In general, the monomodal microporosity with narrow pore size distribution of all the samples presented here were confirmed by a Type I isotherm (67) in the N_2-adsorption experiment. Neither adsorption–desorption hysteresis, nor condensation effects at high values of p/p_0 are observed as exemplarily shown in Fig. 2a for the AMM-Ti_3Si. Figure 2b displays typical pore-size distributions in the micropore region (AMM-Ti_xSi prepared under standard conditions). The pore-size maximum of 0.76 nm with a half width of 0.06 nm (AMM-Ti_{17}Si, Table 3) is comparable to the values known for the crystallographic apertures of 12 membered ring zeolites, such as faujasite (FAU; pore diameter, 0.74) (68). This sorption measurement is remarkable for an amorphous material. The only exception is the pure AMM-Ti, which, in addition to the usual microporosity, reveals a hysteresis pattern indicative of mesoporous bottleneck pores.

Depending on the titania content, the standard materials reveal pore-size maxima between 0.68 nm (AMM-Si) and 0.86 nm (AMM-Ti_{50}Si) with typical halfwidths of 0.05 to 0.1 nm and BET surface areas of 100 (AMM-Ti) to >500 m^2/g (e.g. AMM-Ti_3Si, 523 m^2/g; all data given in Table 3). The decrease in surface area with increasing Ti content can partly be explained by the higher atomic weight of Ti, but most surface area loss must be attributed to an increased contribution of the pure titania character in the high-titania materials. No clear correlation is found between titania content and pore-size maximum, but the distribution tends to be narrow in the range of composition from pure silica up to a balanced composition (Si/Ti = 1 to 100; e.g., AMM-Ti_{50}Si, 0.05 nm halfwidth).

Changes of the sol–gel conditions and of the drying process influence the physisorption data dramatically: The influence of acid-content (without altering the water content) is obvious. BET surface areas rise parallel with an increase in acid concentration from 382 m^2/g (AMM-Ti_3Si, LAC) up to values of 500–600 m^2/g (AMM-Ti_3Si, HAC). Since these surface areas are not significantly higher than that of the HCl/(Si + Ti) ratio of 0.3, the latter is favored for

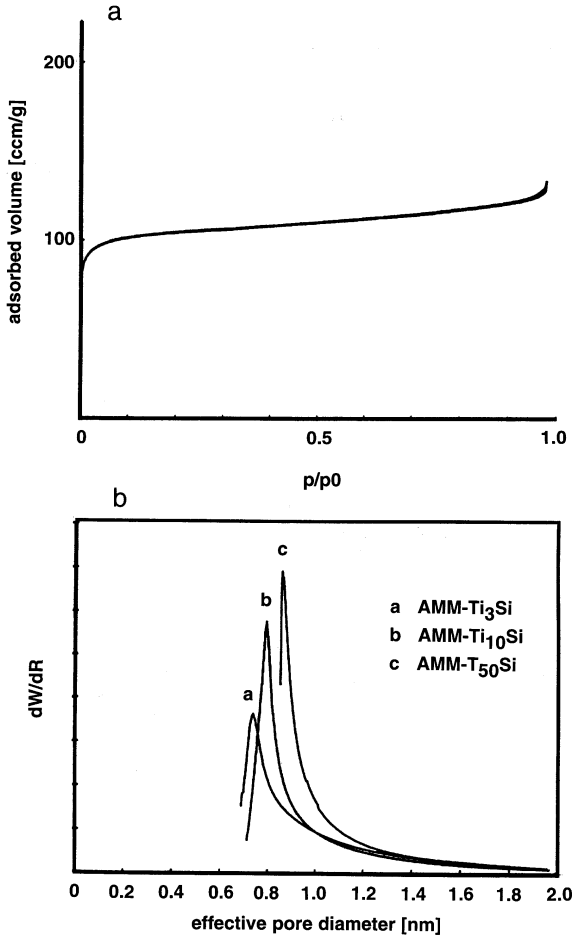

FIG. 2. Typical physisorption results of AMM-Ti_xSi materials. (a) N_2 adsorption–desorption isotherm, (b) pore-size distribution derived from argon adsorption, calculated using the HK-method.

an optimal combination of high surface areas with narrow pore-size distributions (standard conditions).

Sol–gel polycondensation requires theoretically two equivalents of water per alkoxide molecule for complete hydrolysis. As is already known, direct addition of water to a neutral alcoholic solution of TEOS and titanium alkoxide leads to precipitation. Addition of extra water to an acidic alcoholic solution is possible and a clear homogeneous gel is obtained. The effect of the water content on the material sorption properties (AMM-Ti_1Si, HWR) is not affecting the BET surface area of the maximum in pore-size distribution, but a dropping of the micropore volume and a significant broadening of the pore-size distribution (0.08 to 0.15 nm) can be noticed.

Attempts to accelerate the sol–gel process by increasing the gelation temperature or removing the volatiles in vacuum or in a stream of dry gas were not successful. The desired material properties (high surface areas in the pure micropore region, narrow pore-size distribution) are negatively affected by an accelerated procedure. The faster the gelation process, the broader the pore-size distribution and the lower the specific surfaces (AMM-Ti_3Si, G313 and G333). Storing the gels in a flow of dry air or argon causes a severe decrease in surface area (~50%, AMM-Ti_1Si, AD), the effect being even more significant at higher temperatures. Removal of the volatiles under vacuum even results in a low surface material (200 m^2/g, AMM-Ti_9Si, vac.) containing crystalline titania domains, a result consistent with data published recently (69).

A fast calcination is not useful for the preparation of a material with the desired properties, although a higher specific surface is obtained in comparison to the standard materials calcined using a ramped heating (AMM-Ti_{17}Si, FC). A broadening to the pore-size distribution is observed.

Since we did not succeed in reducing the preparation time for the desired materials, we tried to further improve the microstructural features by decelerating the drying process. A slowdown of the evaporation rate of the volatiles by means of closed gelification flasks or storing the solidified samples in a closed system (AMM-Ti_2Si, DD) resulted in slightly increased surface areas with pore size distributions comparable to the gels prepared under standard conditions. Unfortunately, there is not enough data available to justify a detailed explanation of the effects of these sol–gel parameters on the microstructure.

FTIR spectroscopy. For characterization of surface acidity, pyridine adsorption was selected. Figure 3 shows the IR absorbance spectra of Ti–Si mixed oxides with varying composition in their original intensity (left) and in normalized intensities (right, normalized to the band at 1450 cm^{-1}) for better comparison.The region of 1540 cm^{-1} is attributed to the pyridinium ion formed by the adsorption on Brønsted sites, while pyridine coordinated to Lewis sites shows adsorption at 1605, 1580, and 1450 cm^{-1}, respectively (42).

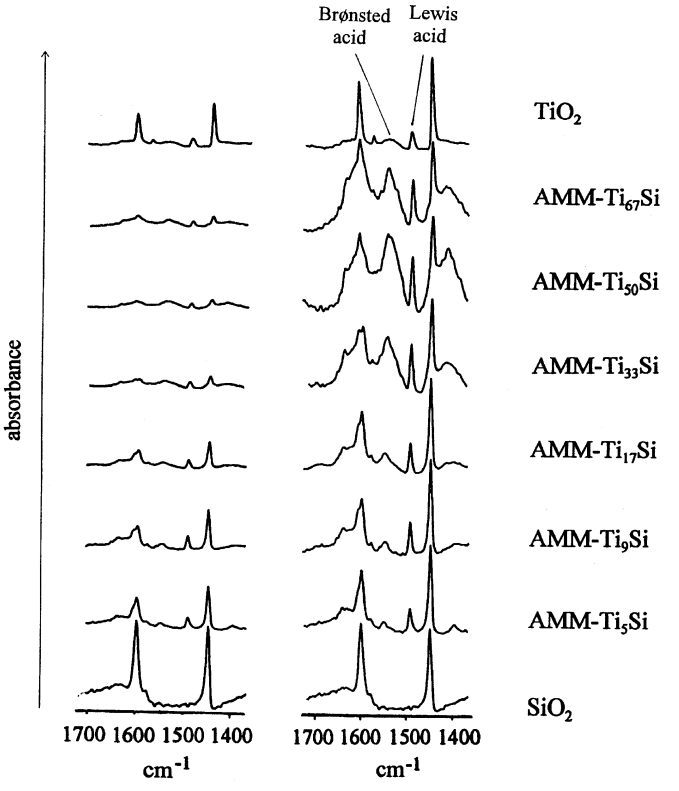

FIG. 3. FTIR absorbance spectra of standard AMM-Ti_xSi materials after pyridine adsorption. Spectra displaying original intensities (left) and intensities normalized to the 1450 cm^{-1} band (right).

We do not interpret the latter, for there might be an overlap with signals attributed to pyridine coordinated to nonacidic OH functions (40).

On all samples the appearance of intense nonacidic silanol bands (1450 and 1595 cm^{-1}) (40) can be seen, indicative of a high density of polar silanol groups in the material. With increasing Ti content the Lewis band at 1605 cm^{-1} grows into the band at 1595 cm^{-1} and becomes dominating at Ti concentrations higher than 33%. A maximum of Brønsted sites is found in the equimolar region of Si/Ti = 1. The band at 1490 cm^{-1} is attributed to Lewis as well as Brønsted sites (40) and is therefore of less importance for the interpretation.

Since titania–silica mixed oxides are important catalysts, catalyst supports, and materials for optical devices, the relationship between microstructure and surface acidity of these glasses has been examined (40–43). The most frequently referred to explanation for the appearence of surface acidity of mixed oxides was given by Tanabe *et al.* (42). They suggest that the coordination numbers of the metal cations in the mixed oxide and in the pure oxides are the same. Furthermore the coordination number of the oxide anions in the mixed oxide should be determined by the oxide that represents the majority. As a consequence a charge difference in the mixture of titania (octahedrally

coordinated) and silica (tetrahedrally coordinated) results. This hypothesis could explain the appearence of Lewis sites on titania-rich mixed oxides (for the impurity cation produces a positive charge difference), while Brønsted acidity should occur on silica-rich mixed oxides (for the negative charge of the impurity cation is balanced by the presence of protons). Recently (43, 45) it was pointed out, that the above-mentioned theory is problematic when applied to Ti–Si-mixed oxides, where Brønsted sites are present on Ti-rich mixed oxides, while Lewis acidity is reduced. In addition, Tanabe's hypothesis cannot explain the significant decrease in total acidity to the Si-rich samples. The authors suggest that there might be Brønsted acidity due to OH groups which compensate for the positive charge on the Ti atoms. Furthermore, they propose that some Ti atoms in the diluted systems isomorphously substitute for Si in tetrahedral coordination, resulting in no charge difference at all. The authors draw the attention to the fact that there is no clear consensus in describing number density and strength of surface acid sites on Ti–Si-mixed oxides, for these are greatly affected by preparation method and material treatment. Our IR results on the AMM materials confirm these conclusions, suggesting a preferred tetragonal incorporation of Ti atoms in the silica-rich materials instead of an octahedral coordination as it is observed in pure TiO_2. In addition, the total intensity of Lewis and Brønsted bands depends on the Ti content.

Microstructural features of the materials were derived from FTIR spectroscopy observed in DRIFT: The incorporation of Ti into a silica matrix results in the appearence of a Si–O–Ti vibration band at 950 cm^{-1}(50), an assignment confirmed by a comparable signal in titanosilasesquioxanes (70). However, in amorphous mixed oxides this band is readily confused by the dominating presence of surface

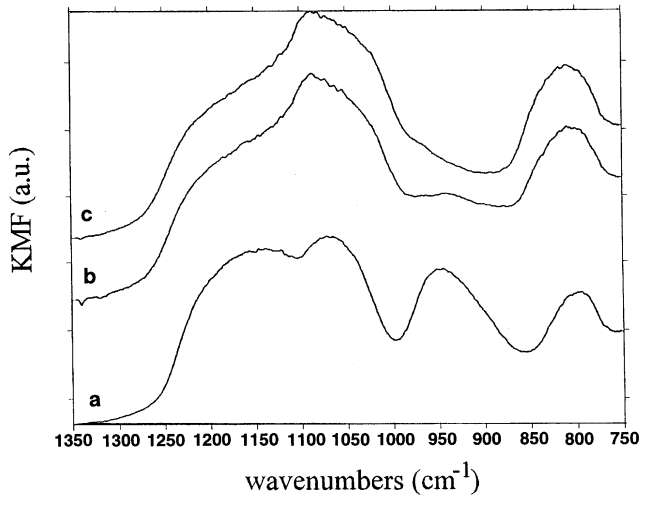

FIG. 4. DRIFT spectra of AMM-Si as function of pretreatment. As synthesized (a), dried in a flow of argon over night at 473 K (b), and dried in a flow of argon over night at 773 K (c).

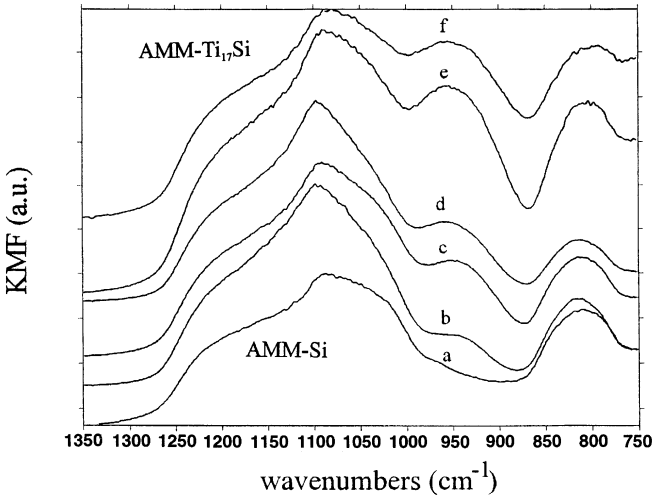

FIG. 5. DRIFT spectra of AMM-Ti_xSi as function of titania content. $X = 0$ (a), 1 (b), 3 (c), 6 (d), 9 (e), and 17 (f). Spectra given in original intensities.

Si–OH groups, which cause a broad absorbance between 920 and 960 cm^{-1}. This silanol band, however, disappears, when the sample is dried at elevated temperatures in a dry atmosphere prior to the measurement. The measurement itself is carried out at room temperature under inert conditions. This drying effect is demonstrated in Fig. 4 with Ti-free silica.

The DRIFT spectra of selected AMM-Ti_xSi samples are given in Fig. 5, clearly demonstrating the relationship between the titania content and the band intensity at approximately 950 cm^{-1}. Semiquantitative evaluation concerning Si–O–Ti-connectivities is possible by the use of Eq. [1] (61). In Fig. 6 the dispersion of titania in the mixed oxides, calculated by Eq. [1] from deconvoluted peak areas, is plotted against the titania content. Obviously, the fraction

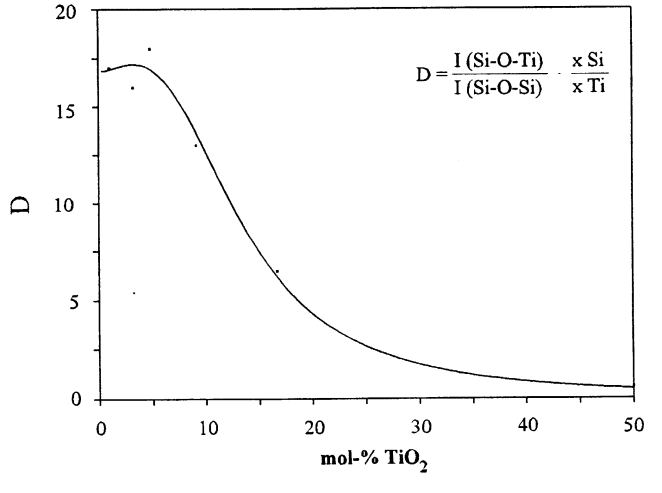

FIG. 6. The *D* value for the Si–O–Ti connectivity as a measure for the titania-dispersion in AMM-Ti_xSi plotted against the titania content.

of the homogeneously dispersed Ti atoms is comparable for AMM-Ti_xSi materials with low Ti content ($x \leqslant 6$). Further increase in the titania content seems to lead to the preferred formation of Ti–O–Ti instead of Si–O–Ti bonds (homocondensation), represented by a decline in the D value, consistent with the other spectroscopic and catalytical results.

Although there should be a correlation between the concentration of surface hydroxyl groups and the hydrophilicity, no such dependence could be derived from the FTIR spectra measured at our conditions. The hydroxyl region of these materials is problematic because of its temperature dependent equilibrium with water addition and release. At our IR conditions (pretreatment at 400°C), the spectral regions between 2000 and 4000 wavenumbers of a hydrophobic TS-1 and a hydrophilic AMM catalyst are identical.

Hydrophobicity measurements. Selective competitive adsorptions of water and octane from the gas phase show significant differences between an AMM-Ti_1Si and TS-1 with a content of 2 mol% of TiO_2. The HI* value of the amorphous oxide is 0.1 (10-fold preference of water over octane), while the silicalite is characterized by a value of 3.3 (3-fold preference of octane over water) under the same analytical conditions. This example shows that the main difference between TS-1 and its amorphous analogues is given by different surface polarities due to the silanol groups on the latter.

UV spectroscopy (DRS). Small amounts of Ti^{4+} in a silicalite lattice result in UV absorption in the region of 45,000 to 48,000 cm^{-1} (35, 37), which has been attributed to the CT band of tetrahedral Ti(IV) (71). In the DRS spectra a strong effect of Ti content on the band position and shape is detected. The Ti-free silica shows no absorption at all, while the Si-free titania reveals an absorption edge around 28,000 cm^{-1}, closely related to the one of anatase. Under ambient conditions, the Ti-containing samples show a bimodal DRS spectrum, where the low wavenumber band between 35,000 and 40,000 cm^{-1} has been assigned to a coordination higher than tetrahedral due to coordination of water and/or alcohol (72). Especially with the low Ti-content materials this band reduces or even disappears after proper predrying of the materials. The spectra of the dry AMM-Ti_1Si to AMM-Ti_9Si mainly show the absorption pattern of isolated, tetrahedral Ti(IV) species in a silica matrix with a single band at ~45,000 cm^{-1} (72). The 45,000 cm^{-1} peak-maximum is shifted to lower wavenumbers with increasing titanium content. The DRS results confirm that Ti(IV) in the amorphous silica matrix is atomically dispersed and tetrahedrally coordinated at contents <9 mol%.

XANES. According to earlier investigations on Ti-containing silicalites (73), the full width half maximum (FWHM) and the position of the Ti-preedge signal structure can be correlated with the coordination sphere of the titanium. Compared to other results in the literature in appearence of nanocrystalline TiO_2 domains can be excluded in the examined AMM-Ti_3Si material, indicating that the Ti is atomically dispersed. The single peak maximum of 3.8 ± 0.2 eV with a relative intensity of 0.34 and a FWHM value of 3.0 ± 0.3 eV suggests that the coordination is not perfectly tetragonal. Compared to corresponding results on Ti silicalites, titanium oxides, and titanium precursors (74–76), the data suggest a five to sixfold coordination on Ti, most likely due to insertion of water or alcohol ligands in agreement with our UV and IR data.

X-ray powder diffraction. An important feature related to the practical potential of heterogeneous catalysts is the thermal stability of the microstructure. The temperature dependent XRDs of the standard AMM materials document the amorphous nature of the mixed oxides <50 mol% titania up to 1173 K. In AMM-$Ti_{50}Si$ the anatase patterns appear during the heating and increase with temperature (Fig. 7). The pure AMM-Ti shows anatase patterns already at low temperatures and starts to transform into rutile at 973 K, the transformation being completed at 1173 K. These results suggest that the low titania materials are mixed on an atomic scale, which prevents the materials from phase separation and crystallisation even at elevated temperatures.

HRTEM/EDX. The high resolution imaging of the mixed oxides (HRTEM) confirms the amorphous character of the materials. Neither electron diffraction patterns typical for crystalline samples nor crystalline lattice fringes are detected in the AMM-Ti_xSi materials. Furthermore, the homogeneity in element distribution was confirmed by the combination of high resolution imaging with energy-dispersive X-ray microanalysis (EDX). The Si/Ti ratios in thin particles are not dependent on the area selected for the point analysis (area range 2 nm to several micrometers) and is identical to the composition of the whole particle.

Catalytic Test Reactions

Catalytic epoxidation of olefines. The catalyzed epoxidations of olefines were carried out at conditions which allowed a comparison of the catalytic properties of the materials as function of preparation conditions and chemical composition. Figure 8 shows the initial rates in epoxidation of 1-octene (displayed as TOF) with TBHP in the presence of AMM-Ti_xSi materials prepared under standard conditions and the final conversion achieved.

There is a dramatic effect of the titania content on the catalytic epoxidation activity (Fig. 8). The lower the Ti content, the higher the number of olefines converted per Ti site. Since the accessible surface areas are comparable for the low titania materials (400–500 m^2/g), the portion of isolated Ti(IV) atoms active for catalysis seems to increase with decreasing Ti content. Since the decrease is most dramatic in the range 0–5% Ti, it cannot be attributed to decreasing

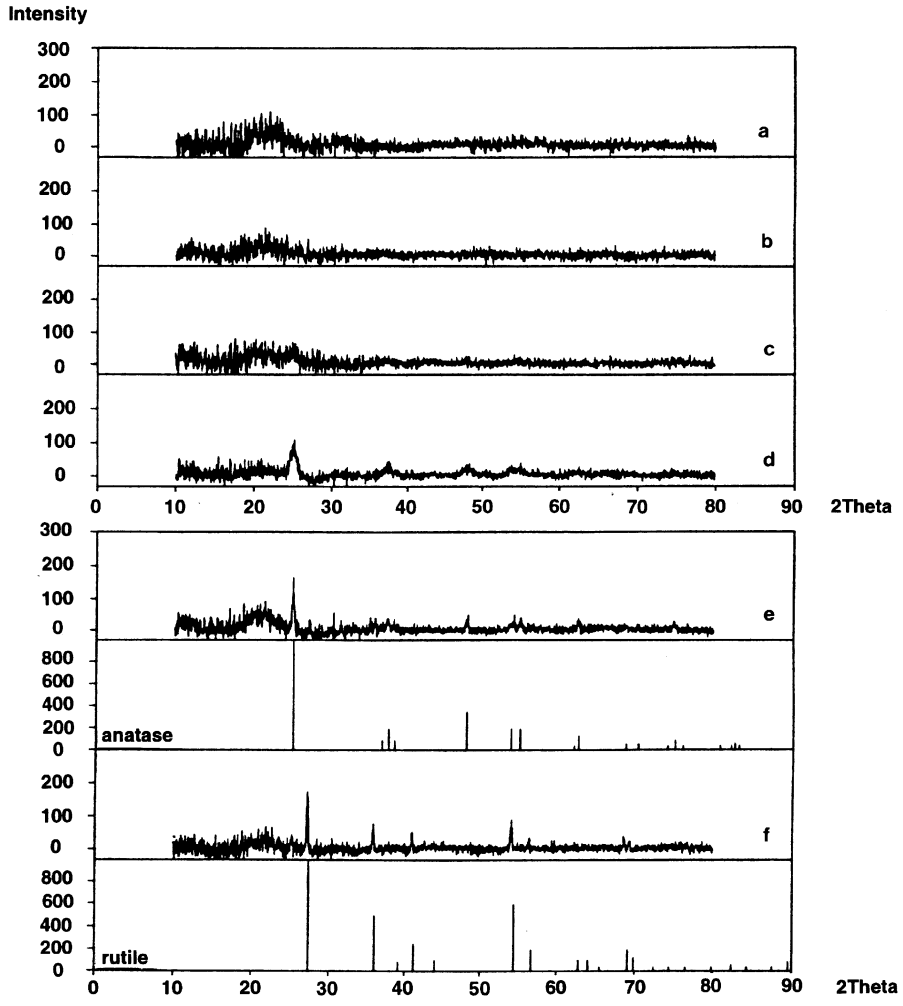

FIG. 7. XRD experiments on AMM-Ti_xSi. (a) AMM-Si, 1173 K; (b) AMM-Ti_3Si, 1173 K; (c) AMM-Ti_{17}Si, 1173 K; (d) AMM-Ti_{50}Si, 1173 K; (e) AMM-Ti, 923 K; and (f) AMM-Ti (1173 K). Patterns of anatase and rutile given for comparison.

dispersion, which is rather constant in this range of Ti content (see Fig. 5). We believe that this decrease is caused by diffusional limitations due to the small pore size, since the absolute conversion (not normalized by the Ti content) over the 0–5% Ti range is the same, indicating that additional Ti centers cannot contribute to the reaction rate. The decrease of final conversion with Ti content >3% may be due to the increasing surface polarity of the material, which would lead to a faster catalyst deactivation by polar molecules. The absolute conversion maximum at our reaction conditions is in the range of 2–3 mol% titania in the mixed oxide. The spent catalysts have been regenerated following the described procedure and were used for the selective oxidations for numerous cycles without a detectable decrease in activity (Fig. 9), indicating that the catalysts deactivate by pore blocking with polar molecules like water or *t*-butanol, as is suggested by the hydrophobicity measurements.

Table 4 also presents the catalysis data for some of the catalysts prepared under nonstandard conditions or with varying chemical compositions (values of representative standard materials from Fig. 8 given for comparison). For example, the epoxidation rate of a low-acid AMM-Ti_3Si is significantly lower than that prepared under standard conditions as well as the one prepared with high amounts of acid, consistent with the accessable BET surface areas. An accelerated gelation and/or drying results in a decrease of activity, since in this case the obtained gels have also a significantly lower surface area than that prepared by the standard procedure. In contrast, the deceleration of the drying process is a suitable means for increasing the epoxidation activities of the gels slightly without causing a significant rise in BET surface area. Apparantely, the obtained three-dimensional structure is more open to access of the substrates due to a broader pore size distribution (half width 0.15 nm).

Unexpected is the high activity of the Ti-ethoxide derived catalysts (AMM-Ti_1Si, TEOT), since this titanium source has been known for its distinctive hydrolysis tendency and

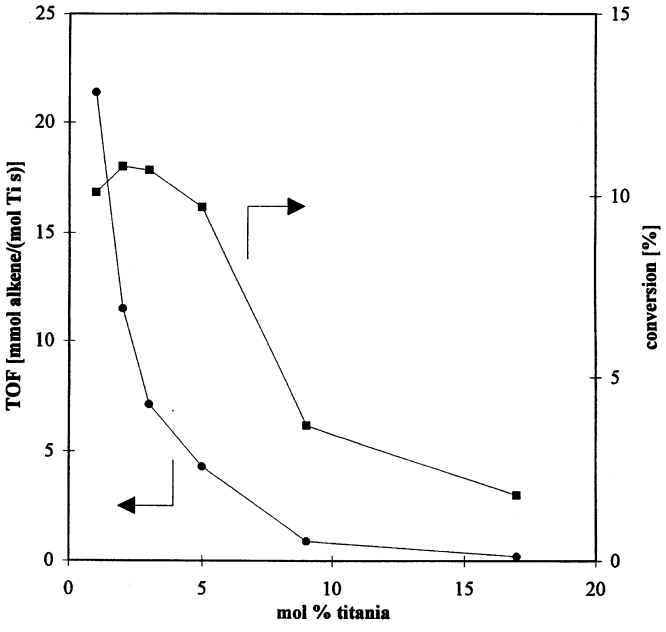

FIG. 8. Final conversions and initial turnover frequencies in catalytic liquid phase epoxidations of 1-octene with TBHP on standard AMM-Ti_xSi materials (test reaction method (i), t_R = 150 min).

TABLE 4

Comparison of Catalytic Alkene Epoxidation on Different AMM–Ti_xSi Materials

Catalyst	Ratio, Si/Ti	Alkene	Method[a]	Conversion[b] (%)	TOF (mmol alkene/ (mol Ti s))
AMM-Ti_1Si	100	1-Octene	i[c]	10.1	21.4
	100	1,3-COD	ii[d]	32.0	20.6
AMM-Ti_2Si	50	1-Octene	i	10.8	11.5
	50	1,3-COD	ii	24.0	7.6
AMM-Ti_3Si	30	1-Octene	i	10.7	7.1
AMM-Ti_9Si	10	1-Octene	i	3.7	0.9
AM-Ti_1Si, TEOT	100	1-Octene	i	9.2	19.5
AMM-Ti_1Si, *i*-PrOH	100	1-Octene	i	10.6	22.5
AMM-Ti_1Si, AD	100	1,3-COD	ii	10.0	6.4
AMM-Ti_2Si, DD	50	1,3-COD	ii	51.0	16.2
AMM-Ti_2Si, HWR	50	1,3-COD	ii	50.0	15.8
AMM-Ti_3Si, G313	30	1-Octene	i	9.9	6.6
AMM-Ti_3Si, G333	30	1-Octene	i	10.4	6.9
AMM-Ti_9Si, vac.	10	1-Octene	i	1.7	0.4
AMM-Ti_9Si, P	10	1-Octene	i	1.8	0.4

[a] As described under Methods.
[b] Reaction time: 150 min.
[c] Method i, max. conversion 18.9%.
[d] Method ii, max. conversion 100%.

also for its ability to catalyze the condensation of Si–OH species (77). Apparently, these properties do not affect this acidic sol–gel process.

For zeolitic Ti-catalysts, increasing epoxidation rates with decreasing olefin size were attributed to significant transport limitation under reaction conditions of epoxidation in the microporous materials (shape selectivity) (38). A similar trend is observed with the AMM-Ti_3Si; the rate of epoxidation of the olefines (epoxide selectivities >98%) decreases with increasing olefin chain length, which points to a zeolite like behaviour of the AMM-systems (34) (see Table 5).

Catalytic selective oxidations of saturated hydrocarbons. The results for the selective oxidation of saturated hydrocarbons such as cyclohexane using TBHP as oxidant can be summarized as follows: AMM-Ti_1Si is a remarkably active catalyst for the oxidation of cyclohexane with TBHP. Without deactivation the highest hydrocarbon conversions are achieved in comparison to other titanium containing materials, such as Ti-MCM-41, Ti-Beta, or TS-1. The main products are cyclohexanol (selectivity, 18.5%), cyclohexanone (selectivity, 46.3%), and adipic acid (selectivity, 32.1%) (78).

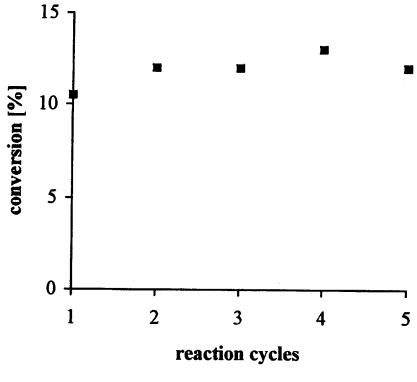

FIG. 9. Regenerability. Catalytic activity (liquid phase epoxidation of 1-octene with TBHP) on AMM-Ti_1Si as function of reaction cycle number (test reaction method (i), t_R = 150 min).

TABLE 5

Rates in Alkene Epoxidation on AMM–Ti_3Si[a]

Alkene	Turnover frequency (mmol alkene/(mol Ti s))
1-Hexene	16.5
1-Octene	8.1
1-Decene	6.3
1-Dodecene	4.7
1-Pentadecene	2.8
Cyclohexene	19.0
Cyclooctene	2.7

[a] Catalytic test reaction following method (i), stopped after 15 min.

SUMMARY

It has been shown, that amorphous microporous Ti–Si-mixed oxides (AMM) can be prepared in a one-step procedure by an acid catalyzed sol–gel process, where Ti incorporation is achieved by simple copolycondensation. The influence of numerous parameters in the one-step preparation on the material properties of the AMM-Ti_xSi has been investigated. High surface area glasses with homogeneous elemental distributions in combination with narrow microporosity were obtained via a strongly acidic alkoxide–sol–gel procedure utilizing stoichiometric amounts of water, followed by a smooth and careful drying and calcination. Surface area, porosity, pore size, pore-size distribution width, and atomic isolation of Ti in the silica matrix of these materials are comparable to that of well known crystalline zeolites. So is the catalytic activity in selective oxidation reactions. The shape selectivities observed in olefin epoxidations is very similar to that known for zeolitic systems. The spectroscopic investigations on the AMM materials underline the microstructural similarity between crystalline Ti-zeolites and the AMM materials. The most significant difference is that crystalline zeolites are effective catalysts utilizing hydrogen peroxide as oxidant, while the amorphous glasses use organic hydroperoxides. This is attributed to the much higher hydrophilicity of the AMM materials due to a large number of surface hydroxyl groups. Also, the AMM catalysts can be often regenerated without loss in activity, indicating high stability as catalysts, again comparable to the Ti-zeolites. In general, the presented AMM-Ti_xSi catalysts are not only a promising alternative to other mixed metal oxides and their application in selective oxidation, they are alternative materials of a supplemental rather than a competitive nature for the rather limited Ti-zeolites.

The study furthermore emphasizes the potential of the sol–gel procedure for the preparation of new large surface area catalytic materials with atomically dispersed catalytically active centers. Pore sizes can be adjusted from mesoporous using supercritical drying techniques (61–63) to microporous by mild acidic polycondensation and controlled drying at ambient conditions. Both methods provide access to well dispersed mixed oxides and in contrast to the traditional catalysts based on defined phases or crystal structures, no limitations of composition and concentration are known. New catalytic properties from yet unknown mixed oxides of well defined pore architecture prepared by the various sol–gel approaches can be expected in the close future.

ACKNOWLEDGMENTS

S.K. thanks the Fonds der Chemischen Industrie and S.T. thanks the CNRS for fellowships. W.F.M. thanks the Fonds der Chemischen Industrie and HOECHST AG for support. We also thank Dr. U. Kolb for the XANES experiments and H. Bretinger for the sorption analyses.

REFERENCES

1. Brinker, C. J., and Scherer, G. W., "Sol-Gel Science." Academic Press, Boston, 1990.
2. Hench, L. L., and West, J. K., *Chem. Rev.* **90**, 33 (1990).
3. Gesser, H. D., and Goswami, P. C., *Chem. Rev.* **89**, 765 (1989).
4. Corriu, R., Leclercq, D., Lefèvre, P., Mutin, P. H., and Vioux, A., *Chem. Mater.* **4**, 961 (1992).
5. Chen, H. D., Tsuchiya, T., and Mackenzie, J. D., *J. Noncryst. Solids* **81**, 227 (1985).
6. Pope, E. J. A., and Mackenzie, J. D., *J. Noncryst. Solids* **87**, 185 (1986).
7. Ying, J. Y., Benzinger, J. B., and Navrotsky, A., *J. Am. Ceram. Soc.* **76**, 2571 (1993).
8. Deng, Z., Breval, E., and Pantano, C. G., *J. Noncryst. Solids* **100**, 364 (1988).
9. Breval, E., Deng, Z., and Pantano, C. G., *J. Noncryst. Solids* **125**, 50 (1990).
10. Gallagher, D., and Ring, T. A., *Chimia* **43**, 298 (1989).
11. Jeng, D. Y., and Rahaman, M. N., *J. Mater. Sci.* **28**, 4964 (1993).
12. van der Pool, A. J. H. P., and van Hoof, J. H. C., *Appl. Catal. A* **92**, 93 (1992).
13. López, T., Herrera, L., Mendez-Viva, J., Bosch, P., Gómez, R., and Gonzalez, R. D., *J. Noncryst. Solids* **147** and **148**, 773 (1992).
14. Cauqui, M. A., Calvino, J. J., Cifredo, G., Esquivias, L., and Ródriguez-Izquierdo, J. M., *J. Noncryst. Solids* **147** and **148**, 758 (1992).
15. Carati, A., Davini, E., Clerici, M. G., and Bellussi, G., European patent application EP 492,697, 1992.
16. Sohn, J. R., and Jang, H. J., *J. Catal.* **132**, 563 (1991).
17. Itoh, M., Hattori, H., and Tanabe, K., *J. Catal.* **35**, 225 (1974).
18. Neumann, R., and Levin-Elad, M., *Appl. Catal. A* **122**, 85 (1995).
19. Heilmann, J., and Maier, W. F., *Angew. Chem.* **106**, 491 (1994).
20. Diré, S., Babonneau, F., Carturan, G., and Livage, J., *J. Noncryst. Solids* **147** and **148**, 62 (1992).
21. Dislich, H., and Hinz, P., *J. Noncryst. Solids* **48**, 11 (1982).
22. De, G., Kundu, D., Karmakar, B., and Ganguli, D., *J. Noncryst. Solids* **122**, 211 (1990).
23. Ellsworth, M. W., and Novak, B. M., *Chem. Mater.* **5**, 839 (1993).
24. Kaiser, A., and Schmidt, H., *J. Noncryst. Solids* **63**, 261 (1994).
25. Xu, Q., and Anderson, M. A., *J. Am. Ceram. Soc.* **76**, 2093 (1993).
26. Maier, W. F., Tilgner, I.-C., Wiedorn, M., and Ko, H.-C., *Adv. Mater.* **5**, 726 (1993).
27. Maier, W. F., Tilgner, I.-C., Wiedorn, M., Ko, H.-C., Ziehfreund, A., and Sell, R., *Adv. Mater.* **5**, 730 (1993).
28. Thorimbert, S., Klein, S., and Maier, W. F., *Tetrahedron* **51**, 3787 (1995).
29. Maschmeyer, T., Rey, F., Sankar, G., and Thomas, J. M., *Nature* **378**, 159 (1995).
30. Maier, W. F., Martens, J. A., Klein, S., Heilmann, J., Parton, R., Vercruysse, K., and Jacobs, P. A., *Angew. Chem.* **108**, 222 (1996).
31. Sheldon, R. A., and Dakka, J., *Catal. Today* **19**, 215 (1994).
32. Sheldon, R. A., and Kochi, J. K., "Metal-Catalyzed Oxidations of Organic Compounds." Academic Press, New York, 1981.
33. Taramasso, M., Perego, G., and Notari, B., US Patent 4,410,501, (1983).
34. Reddy, J. S., Kumar, R., and Ratnasamy, P., *Appl. Catal.* **58**, L1 (1990).
35. Camblor, M. A., Corma, A., Martínez, A., and Pérez-Pariente, J., *J. Chem. Soc. Chem. Comm.*, 589 (1992).
36. Tanev, P. T., Chibwe, M., and Pinnavaia, T. J., *Nature* **368**, 321 (1994).
37. Jacobs, P. A., *in* "Selective Oxidations in Petrochemistry, Tagungsbericht 9204, Proceedings of the DGMK-Conference, 1992, Goslar, Germany" (M. Baerns and J. Weitkamp, Eds.), p. 171. DGMK, Hamburg, 1992.
38. Corma, A., Esteve, P., Martínez, A., and Valencia, S., *J. Catal.* **152**, 18 (1995).
39. Khouw, C. B., Dartt, C. B., Labinger, J. A., and Davis, M. E., *J. Catal.* **149**, 195 (1994).

40. Odenbrand, C. U. I., Brandin, J. G. M., and Busca, G., *J. Catal.* **135**, 505 (1992).
41. Tanabe, K., Sumiyoshi, T., Shibata, K., Kiyoura, T., and Kitagawa, J., *Bull. Chem. Soc. Jpn.* **47**, 1064 (1974).
42. Tanabe, K., *in* "Catalysis—Science and Technology" (J. R. Anderson and M. Boudart, Eds.), Vol. 2, p. 231. Springer, Berlin, 1981.
43. Liu, Z., Tabora, J., and Davis, R. J., *J. Catal.* **149**, 117 (1994).
44. Terabe, K., Kato, K., Miyazaki, H., Yamaguchi, S., Imai, A., and Iguchi, Y., *J. Mater. Sci.* **29**, 1617 (1994).
45. Liu, Z., and Davis, R. J., *J. Phys. Chem.* **98**, 1253 (1994).
46. Miranda Salvado, I. M., Margaça, F. M. A., and Teixera, J., *J. Noncryst. Solids* **163**, 115 (1993).
47. Cheng, J. J., and Wang, D. W., *J. Noncryst. Solids* **100**, 288 (1988).
48. Sakka, S., and Kamiya, K., *J. Noncryst. Solids* **42**, 403 (1980).
49. Wang, B., and Wilkes, G. L., *J. Polym. Sci., Polym. Chem.* **29**, 905 (1991).
50. Aizawa, M., Nosaka, Y., and Fujii, N., *J. Noncryst. Solids* **128**, 77 (1991).
51. Beghi, M., Chiudo, P., Costa, L., Palladino, M., and Pirini, M. F., *J. Noncryst. Solids* **145**, 175 (1992).
52. Yoldas, B. E., *J. Noncryst. Solids* **38**, 81 (1980).
53. Zhu, C., Hou, L., Gan, F., and Jiang, Z., *J. Noncryst. Solids* **63**, 105 (1984).
54. Barboux-Doeuff, S., and Sanchez, C., *Mat. Res. Bull.* **29**, 1 (1994).
55. Livage, J., and Sanchez, C., *J. Noncryst. Solids* **145**, 11 (1992).
56. Diré, S., and Babonneau, F., *J. Noncryst. Solids* **167**, 29 (1994).
57. Doeuff, S., Henry, M., Sanchez, C., and Livage, J., *J. Noncryst. Solids* **89**, 206 (1987).
58. Sanchez, C., Livage, J., Henry, M., and Babonneau, F., *J. Noncryst. Solids* **100**, 65 (1988).
59. Doeuff, S., Henry, M., and Sanchez, C., *Mat. Res. Bull.* **25**, 1519 (1990).
60. Notari, B., *Stud. Surf. Sci. Catal.* **37**, 413 (1988).
61. Dutoit, D. C. M., Schneider, M., and Baiker, A., *J. Catal.* **153**, 165 (1995).
62. Hutter, R., Mallat, T., and Baiker, A., *J. Catal.* **153**, 177 (1995).
63. Hutter, R., Dutoit, D. C. M., Mallat, T., Schneider, M., and Baiker, A., *J. Chem. Soc. Chem. Comm.*, 163 (1995).
64. Tilgner, I.-C., Fischer, P., Bohnen, F. M., Rehage, H., and Maier, W. F., *Microporous Mater.* **5**, 77 (1995).
65. Kubelka, P., and Munk, F., *Z. Tech. Phys.* **12**, 593 (1931).
66. Berke, C. H., Kiss, A., Kleinschmit, P., and Weitkamp, J., *Chem.-Ing. Tech.* **63**, 623 (1991).
67. Jovanoviç, D. S., *Kolloid-Z., Z. Polym.* **23**, 1214 (1969).
68. Meier, W. M., and Olson, D. H., "Atlas of Zeolite Structure Types." Butterworths, London, 1992.
69. Sakata, T., Mori, H., and Yoneyama, H., *Chem. Lett.* 653 (1994).
70. Winkhofer, N., Voigt, A., Dorn, H., Roesky, H. W., Steiner, A., Stalke, D., and Reller, A., *Angew. Chem.* **106**, 1414 (1994).
71. Zecchina, A., Spoto, G., Bordiga, S., Ferrero, A., Petrini, G., Leofanti, G., and Padoran, M., *Stud. Surf. Sci. Catal.* **69**, 251 (1991).
72. Klein, S., Maier, W. F., Weckhuysen, B. M., Martens, J. A., and Jacobs, P. A., *J. Catal.* **163**, 489 (1996).
73. Bordiga, S., Coluccia, S., Lambert, C., Marchese, L., Zecchina, A., Boscherini, F., Buffa, F., Genoni, F., Leofanti, G., Petrini, G., and Vlaic, G., *J. Phys. Chem.* **98**, 4125 (1994).
74. Trong On, D., Bonneviot, L., Bittar, A., Sayari, A., and Kaliaguine, S., *J. Mol. Catal.* **74**, 233 (1992).
75. Lopez, A., Tuilier, M. H., Guth, J. L., Delmotte, L., and Popas, J. M., *J. Solid State Chem.* **102**, 480 (1993).
76. Babonneau, F., Doeuff, S., Leaustic, A., Sanchez, C., Cartier, C., and Verdaguer, M., *Inorg. Chem.* **27**, 3166 (1988).
77. Lin, C. C., and Basil, J. D., *Mater. Res. Soc. Symp. Proc.* **73**, 585 (1986).
78. Klein, S., Martens, J. A., Parton, R., Vercruysse, K., Jacobs, P. A., and Maier, W. F., *Catal. Lett.* **38**, 209 (1996).